NASA TECHNICAL NOTE

NASA TN D-6729

NASA TN D-6729

ANALYTICAL CORRELATION OF CENTRIFUGAL COMPRESSOR DESIGN GEOMETRY FOR MAXIMUM EFFICIENCY WITH SPECIFIC SPEED

by Michael R. Galvas

Lewis Research Center
Cleveland, Ohio 44135

NATIONAL AERONAUTICS AND SPACE ADMINISTRATION • WASHINGTON, D. C. • MARCH 1972

1. Report No.	2. Government Accession No.	3. Recipient's Catalog No.
NASA TN D-6729		

4. Title and Subtitle	5. Report Date
ANALYTICAL CORRELATION OF CENTRIFUGAL COMPRESSOR DESIGN GEOMETRY FOR MAXIMUM EFFICIENCY WITH SPECIFIC SPEED	March 1972
	6. Performing Organization Code
7. Author(s) Michael R. Galvas	8. Performing Organization Report No. E-6638
	10. Work Unit No. 132-15
9. Performing Organization Name and Address Lewis Research Center National Aeronautics and Space Administration Cleveland, Ohio 44135	11. Contract or Grant No.
	13. Type of Report and Period Covered Technical Note
12. Sponsoring Agency Name and Address National Aeronautics and Space Administration Washington, D.C. 20546	14. Sponsoring Agency Code

15. Supplementary Notes

16. Abstract

Centrifugal compressor performance was examined analytically to determine optimum geometry for various applications as characterized by specific speed. Seven specific losses were calculated for various combinations of inlet tip-exit diameter ratio, inlet hub-tip diameter ratio, blade exit backsweep, and inlet-tip absolute tangential velocity for solid body prewhirl. The losses considered were inlet guide vane loss, blade loading loss, skin friction loss, recirculation loss, disk friction loss, vaneless diffuser loss, and vaned diffuser loss. Maximum total efficiencies ranged from 0.497 to 0.868 for a specific speed range of 0.257 to 1.346. Curves of rotor exit absolute flow angle, inlet tip-exit diameter ratio, inlet hub-tip diameter ratio, head coefficient and blade exit backsweep are presented over a range of specific speeds for various inducer tip speeds to permit rapid selection of optimum compressor size and shape for a variety of applications.

17. Key Words (Suggested by Author(s))

Centrifugal compressor
Efficiency
Specific speed

18. Distribution Statement

Unclassified - unlimited

19. Security Classif. (of this report)	20. Security Classif. (of this page)	21. No. of Pages	22. Price*
Unclassified	Unclassified	38	$3.00

* For sale by the National Technical Information Service, Springfield, Virginia 22151

ANALYTICAL CORRELATION OF CENTRIFUGAL COMPRESSOR DESIGN GEOMETRY FOR MAXIMUM EFFICIENCY WITH SPECIFIC SPEED

by Michael R. Galvas

Lewis Research Center

SUMMARY

Centrifugal compressor performance was examined analytically to determine optimum geometry for various applications as characterized by specific speed. Seven specific losses were calculated for various combinations of inlet tip-exit diameter ratio, inlet hub-tip diameter ratio, blade exit backsweep, and inlet tip absolute tangential velocity for solid body prewhirl. The losses considered were inlet guide vane loss, blade loading loss, skin friction loss, recirculation loss, disk friction loss, vaneless diffuser loss, and vaned diffuser loss. Maximum total efficiencies ranged from 0.497 to 0.868 for a specific speed range of 0.257 to 1.346.

Curves of rotor exit absolute flow angle, inlet tip-exit diameter ratio, inlet hub-tip diameter ratio, head coefficient, and blade exit backsweep are presented over a range of specific speeds for various inducer tip speeds to permit rapid selection of optimum compressor size and shape for a variety of applications.

INTRODUCTION

Centrifugal compressors are suitable for aircraft, space-power systems, and other applications where small, compact power systems are a necessity. Because the overall geometry for each application could vary greatly, it would be advantageous to have a method whereby the optimum geometry could be systematically selected. One parameter that roughly correlates efficiency with application is specific speed, a term which has traditionally been used in the analysis of pumps and compressors.

Specific speed is a term which relates compressor rotative speed, flow rate, and ideal enthalpy rise. Impellers associated with a large total head and low flow rate are characterized by a low specific speed and, conversely, those with a low total head and high flow rate are characterized by a high specific speed. Many combinations of

velocity diagram characteristics and compressor geometric parameters are possible at a particular specific speed. The combinations of greatest interest are those that will result in the maximum attainable efficiency at a particular specific speed.

Several previous studies have investigated specific speed and its relation to attainable efficiency. Balje (ref. 1) presented plots of efficiency as a function of specific speed and specific diameter. Specific diameter is a term relating impeller exit diameter, adiabatic head, and inlet volume flow rate. From his study it was concluded that, for centrifugal compressors with swirl-free inlets, maximum efficiency could be expected for backswept impellers with specific speeds in the range of 0.705 to 1.018. The optimum exit-inlet diameter ratio was mainly a function of specific diameter. Maximum attainable efficiency decreased with decreasing specific speed because of gas density changes related to high pressure ratios encountered in low specific speed machines. The additional losses incurred are due primarily to increased skin friction and disk friction.

Nichols, McPherson, and Balje (ref. 2) investigated specific-speed - efficiency characteristics of centrifugal pumps through an analytical determination of losses. Their principal findings were that maximum efficiency increased with increasing specific diameter, that maximum efficiency was not particularly sensitive to impeller inlet hub-tip radius ratio, and that maximum efficiency could be expected for backswept impeller blades.

The general expression of specific speed may be expanded so that several of the geometric parameters of interest appear explicitly in the equation. Examination of the equation shows that many combinations of the parameters are possible at a given specific speed. The combinations of greatest interest are those that will result in maximum attainable total efficiency at a particular specific speed. The present study is an analytical correlation of maximum total efficiency with specific speed by a calculation of specific losses that are dependent on geometric parameters and velocity diagram characteristics. The method is a one-dimensional analysis conducted at fixed inlet conditions of gas state and inducer tip speed. All calculations were made for air entering the compressor at U.S. standard sea-level conditions. Geometric parameters and velocity characteristics considered in the study were inlet prewhirl, impeller inlet absolute critical velocity ratio, inlet tip-exit diameter ratio, blade backsweep at the impeller exit, and inlet hub-tip diameter ratio. Losses considered were those resulting from inlet guide vanes if prewhirl was incorporated into the impeller design, impeller blade loading, skin friction, recirculation of the working fluid between the vaned diffuser and impeller, diffusion in the vaneless space, and diffusion in the vaned diffuser.

Results of this study show the values of geometric variables and velocity diagram characteristics that result in maximum efficiency at a given specific speed in the range investigated. Individual losses are presented to indicate the changes in loss distribution with specific speed along the curves of maximum total efficiency.

METHOD OF ANALYSIS

Approach

Specific speed, a term relating shaft rotative speed, inlet flow volume, and ideal work is defined as

$$N_S \equiv \frac{\omega\sqrt{Q_1}}{H_{id}^{3/4}} \tag{1}$$

Compressor station numbers are shown in figure 1, and all symbols are defined in appendix A. Equation (1) can be expanded into

$$N_S = \pi^{1/2}\psi^{-3/4}\left(\frac{V_{1m}}{u_{1T}}\right)^{1/2}\left(\frac{D_{1T}}{D_2}\right)^{3/2}\left(1 - \lambda^2\right)^{1/2} \tag{2}$$

which shows that a number of combinations of geometric variables and velocity diagram parameters are possible at a given specific speed. Thus, the problem is to determine the combination at a specific speed that will yield maximum efficiency. Individual losses were computed for each combination of independent variables considered. The extensive range of these combinations results in a variety of different configurations at a particular specific speed. Losses considered were those due to inlet guide vanes, blade loading, skin friction, disk friction, recirculation, vaneless space diffusion, and vaned diffuser diffusion. At the inlet triangles were calculated from a specified absolute critical velocity ratio and amount of solid-body prewhirl at the inducer tip (see fig. 2). Gradients in axial component of absolute velocity were calculated to satisfy radial equilibrium. At the exit relative velocity was assumed to deviate from the blade with a slip velocity calculated by the method of reference 3. With the magnitude of relative velocity known from a constraint on relative velocity ratio, impeller velocity known from exit-inlet tip diameter ratio, specified impeller inlet tip speed, and blade exit angle, the exit triangle was then calculated.

Impeller actual aerodynamic work imparted to the fluid was calculated with the rms inlet prewhirl velocity and blade speed and the exit absolute tangential velocity and blade speed. Actual shaft work input was determined by adding disk friction and recirculation losses to the impeller actual aerodynamic work. The disk friction and recirculation work was arbitrarily assumed to escape the system through heat transfer. Isentropic

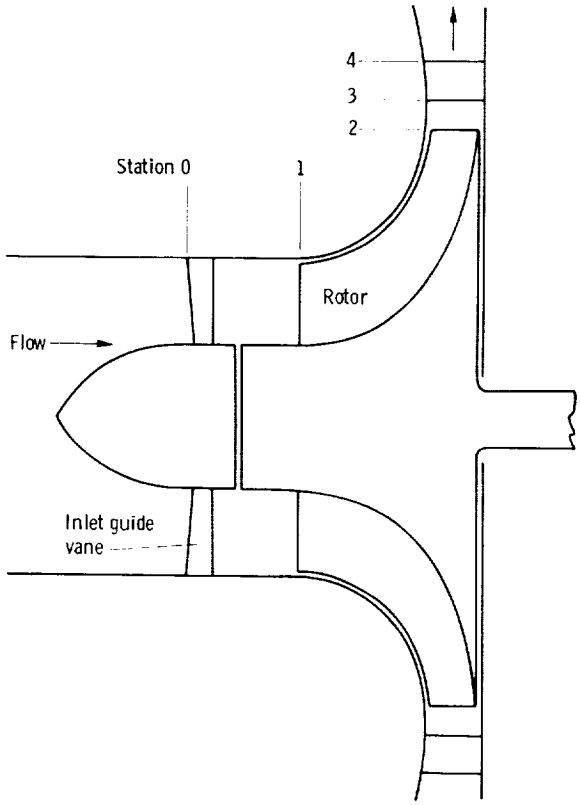

Figure 1. - Meridional cross section of compressor.

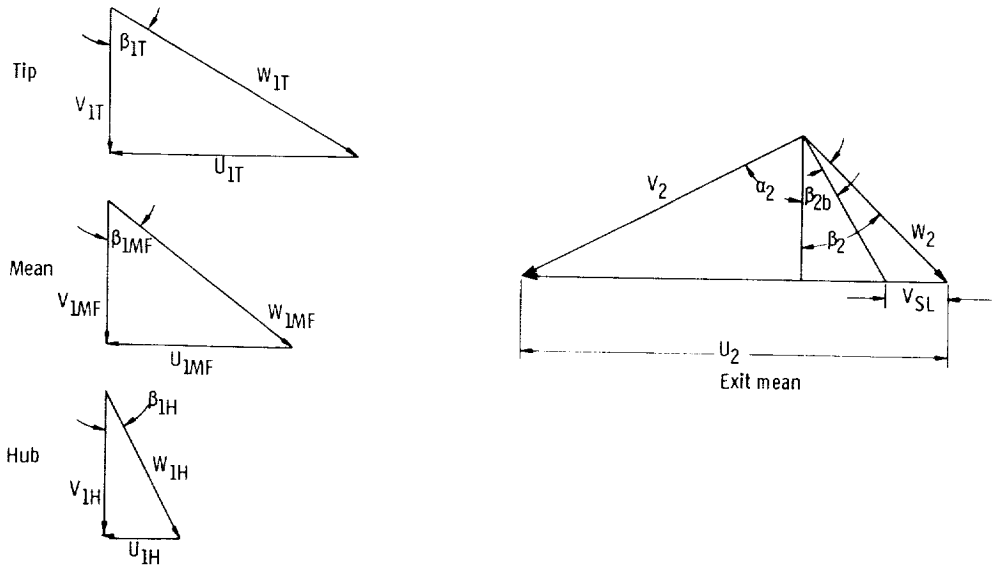

Figure 2. - Velocity diagrams.

work, which is the work associated with the actual pressure ratio attained, was calculated as the actual work minus the summation of internal losses. Adiabatic efficiency was calculated as isentropic work divided by actual work.

Impeller exit geometry was determined from actual aerodynamic work, internal impeller losses, and the constraint on inducer tip-exit relative velocity ratio.

Calculated Losses

Inlet guide vane loss. - Equations relating working fluid kinetic energy level, boundary layer, and blade geometry were developed for axial turbine stators and rotors in reference 4. It was assumed that the term for turbine stators was applicable to inlet guide vanes of a centrifugal compressor and the relevant component of the total loss was used for the guide vane calculations. This equation was evaluated at mean inlet conditions:

$$\Delta h_{IGV} = \frac{0.4}{2Re^{0.2} \cot \alpha_{1MF}} \left(V_0^2 + V_{1MF}\right) \tag{3}$$

Blade loading loss. - Boundary-layer growth in the impeller is highly dependent on the internal diffusion of the working fluid. It has been found (ref. 5) that low loss blade loadings are those that are characterized by rapid deceleration in the inducer and highly loaded inducers in comparison to the outlet. These criteria tend to minimize losses associated with secondary flows and separation in the impeller. Reference 6 proposed an equation for calculating the diffusion factor of the impeller based on a uniform velocity loading along the blade chord. With the diffusion factor calculated by this method, the loss due to blade loading was expressed as

$$\Delta h_{BL} = 0.05 D_f^2 u_2^2 \tag{4}$$

Skin friction loss. - In addition to the losses resulting from flow separation and secondary flows, the impeller incurs losses due to skin friction of the wetted area of the impeller and shroud. Reference 6 proposed an equation for this loss based on pipe friction for fully developed turbulent flow:

$$\Delta h_{SF} = 5.6 C_f \frac{\frac{L}{D_2}}{\frac{D_{hyd}}{D_2}} \left(\frac{W}{u_2}\right)_{av}^2 u_2^2$$

Disk friction loss. - Windage loss on the compressor back-face was calculated using the equation

$$\Delta h_{DF} = 0.01356 \frac{\rho_2}{wRe^{0.2}} u_2^3 D_2^2 \tag{6}$$

which is a form of the disk friction power loss found in reference 7.

Recirculation loss. - Losses incurred through the additional work done on the working fluid due to back-flow from the vaned diffuser to impeller was expressed as

$$\Delta h_{RC} = u_2^2 \, 0.02(\tan \alpha_2)^{1/2} D_f^2 \tag{7}$$

This is a modification of the loss estimate proposed in reference 6.

Vaneless diffuser loss. - Between the rotor and vaned diffuser a vaneless space was used to decelerate the flow to Mach 0.8. This was done as a precaution against shock flow in the diffuser vanes. Flow angle and Mach number variation with increasing radius were determined by numerical solution of the governing differential equations developed in reference 8. Total pressure distribution was calculated using the equation developed in reference 6. When fluid properties had been determined at the vaned diffuser leading-edge radius the vaneless diffuser loss was calculated from the equation:

$$\Delta h_{VLD} = C_p T_2' \left[\left(\frac{p_3}{p_3'} \right)^{(\gamma-1)/\gamma} - \left(\frac{p_3}{p_2'} \right)^{(\gamma-1)/\gamma} \right] \tag{8}$$

Vaned diffuser loss. - Curves of maximum static pressure recovery coefficient at a given area ratio were extrapolated from the test data for square throat diffusers reported in reference 9 for various combinations of vaned diffuser throat Mach number, blockage, and area ratio. Vaned diffuser area ratio and pressure recovery coefficient C_p^{**} corresponding to an exit Mach number of 0.2 were established through iteration. With the exit static and total pressures established by this method, vaned diffuser head loss was calculated by

$$\Delta h_{VD} = C_p T_2' \left[\left(\frac{p_4}{p_4'} \right)^{(\gamma-1)/\gamma} - \left(\frac{p_4}{p_3'} \right)^{(\gamma-1)/\gamma} \right] \tag{9}$$

Procedure

The initial set of performance calculations was made at a fixed inlet absolute critical velocity ratio of 0.3 and inducer tip critical velocity ratio of 0.520. Subsequent calculations were made at inlet absolute critical velocity ratios of 0.2, 0.4, and 0.7 with corresponding inducer tip critical velocity ratios of 0.346, 0.693, and 1.212, respectively. These additional calculations were made to study the effects of internal velocity level on compressor performance. For all the calculations, inlet total pressure, total temperature, total dynamic viscosity, gas constant, and ratio of specific heats were held constant. All calculations were made for air as the working fluid at U.S. standard sea-level conditions. Inducer tip-exit relative velocity ratio was held constant at 0.7. Low values of relative velocity ratio may result in highly separated flow in the rotor, in which case the empirical loss estimates would be extremely questionable. Maximum inlet absolute tangential velocity for the prewhirl cases was limited to 0.4 of the inducer tip speed. Values greater than 0.4 resulted in inducer velocity diagrams that were not of interest in this study.

The geometric parameters and velocity diagram characteristics D_{1T}/D_2, β_{2b}, V_{1T}/V_{cr}, λ, and $V_u/u\,|_1$ were varied over the following ranges:

$$0.3 \leq \frac{D_{1T}}{D_2} \leq 0.7$$

$$0^{\circ} \leq \beta_{2b} \leq 45^{\circ}$$

$$0.3 \leq \lambda \leq 0.7$$

$$0 \leq \left.\frac{V_u}{u}\right|_1 \leq 0.4$$

$$0.2 \leq \frac{V_{1T}}{V_{cr}} \leq 0.7$$

Inducer tip-exit diameter ratio was varied between 0.3 and 0.7 to attain the range of specific speeds investigated. Minimum inducer hub-tip diameter ratio was set at 0.3 since manufacturing and blockage problems are encountered with low values of this variable. Maximum inducer hub-tip diameter ratio was set at 0.7. Impeller exit blade backsweep range of 0° to 45° included the maximum efficiency configuration at every specific

speed. Vaned diffuser inlet Mach number was limited to 0.8. A conservative subsonic limit was placed on the diffuser inlet Mach number in anticipation of shock-free vaned diffuser performance. Vaned diffuser exit Mach number was set at 0.2 since this represents a desirable combustor inlet velocity.

Since efficiency and specific speed were of primary interest among the output variables, the calculations were evaluated in these terms. The broad range of input variables resulted in a wide spread in specific speeds and an appreciable spread in efficiencies at each specific speed. The upper envelope of curves of efficiency as a function of specific speed therefore represents the curve of optimum geometry. After this curve had been determined, calculated points on or near it were examined for definition of optimum geometry.

RESULTS

Efficiency Characteristics

Rotor inlet tip speed was held constant at a critical velocity ratio of 0.520 for the base set of performance calculations with air entering the compressor at U.S. standard sea-level conditions. Subsequent calculations were made at rotor inlet tip critical velocity ratios of 0.346, 0.693, and 1.212. The combinations of input variables resulted in maximum total efficiencies ranging from 0.497 to 0.868 and specific speeds from 0.257 to 1.346. Figure 3 shows the variation in maximum total efficiency with specific speed and rotor inlet tip speed. The geometric parameters that resulted in these curves were examined for definition of optimum geometry. The wide range of specific speeds attained with the subsonic inducer tip speeds was not attained with the transonic inducer tip speed because the maximum inducer tip-exit diameter ratio for this configuration was limited to 0.5. This results in an impeller exit tip speed of 752 meters per second. Higher values were considered to be unreasonable for this study. The large difference in attainable maximum total efficiency for the transonic inducer in comparison with the subsonic inducers is due primarily to losses associated with the vaneless and vaned diffusers.

Compressor Geometry and Velocity Diagram Characteristics

Compressor geometry was examined for calculated points on or near the curve of maximum total efficiency. Several design parameters were then plotted as functions of specific speed to reflect the changes in optimum compressor shape with specific speed.

Figure 4 shows the variation in rotor exit absolute flow angle for a swirl-free inlet

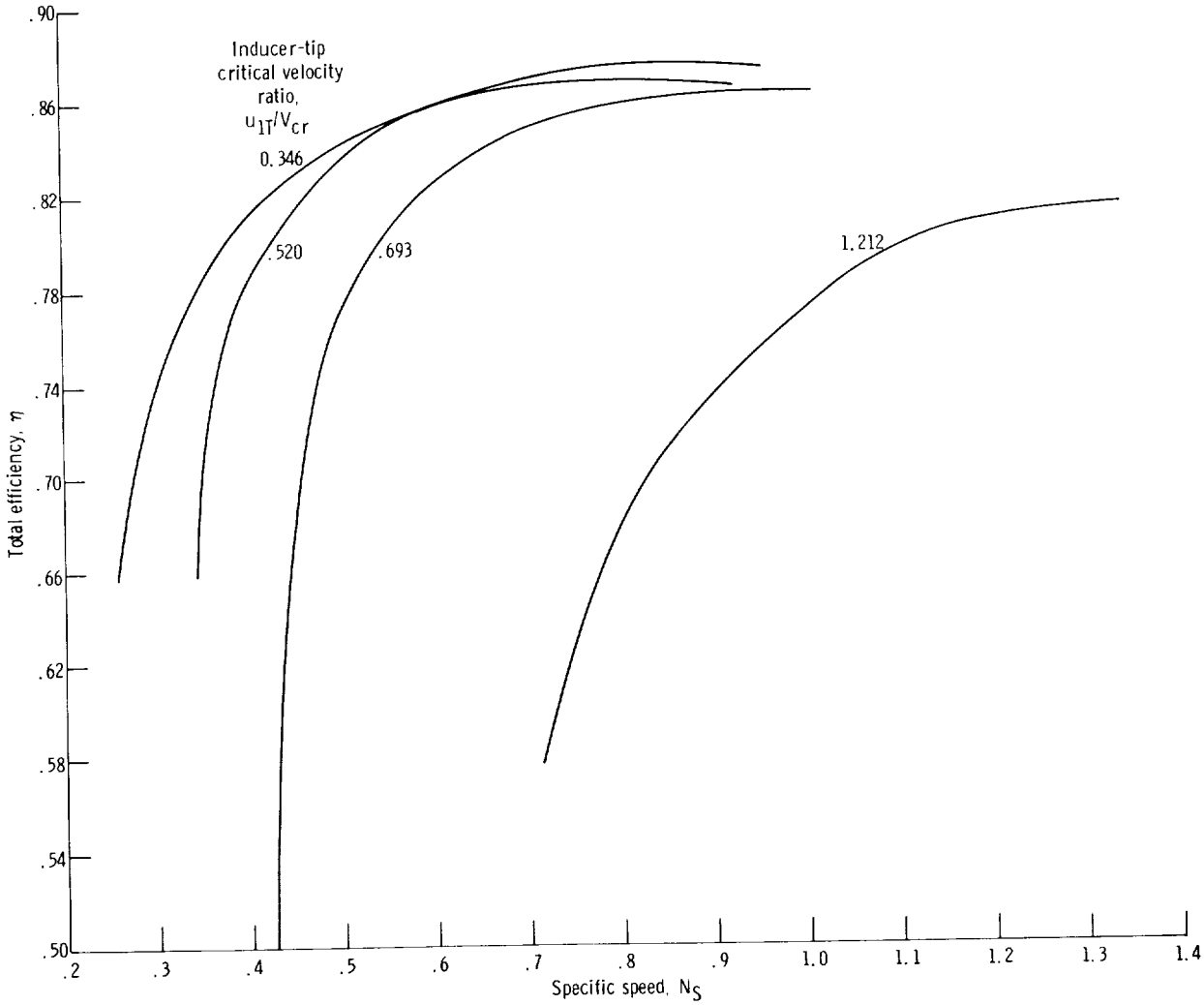

Figure 3. - Variation in maximum total efficiency with specific speed and inducer tip speed.

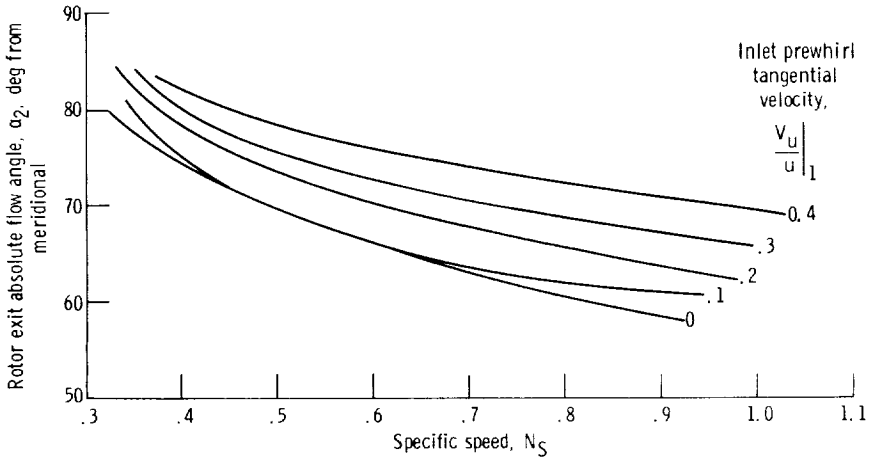

Figure 4. - Variation in optimum rotor exit absolute flow angle with specific speed at various inlet prewhirl tangential velocities. Inducer tip critical velocity ratio, 0.520.

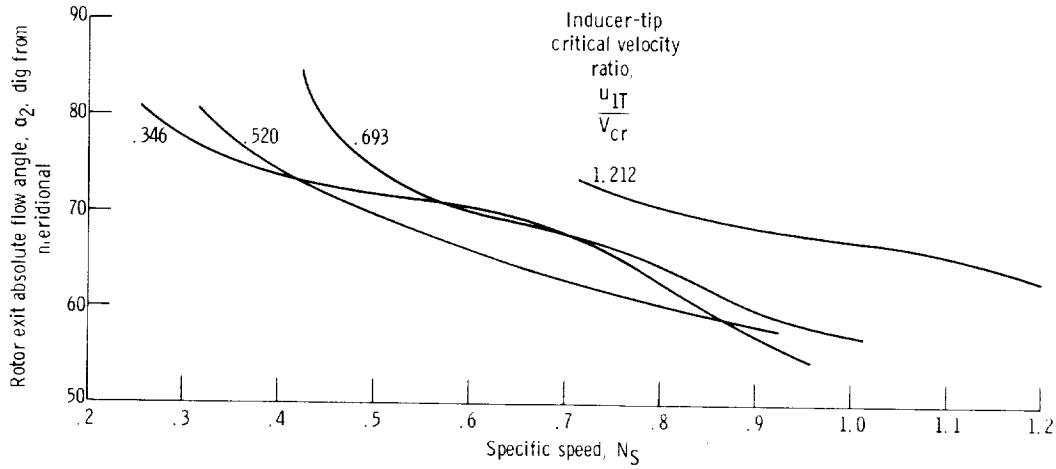

Figure 5. - Variation in optimum rotor exit absolute flow angle with specific speed at various inducer tip speeds.

and four values of solid-body prewhirl for the inducer tip critical velocity ratio of 0.520.

The variation in optimum rotor exit absolute flow angle with specific speed and inducer tip speed is shown in figure 5. The optimum rotor exit absolute flow angle generally increased at a given specific speed with increased inducer tip speeds. This resulted from higher values of optimum backsweep associated with higher inducer tip speeds.

Figure 6 shows the variation in optimum inducer hub-tip diameter ratio with specific speed for the four inducer tip speeds considered. For the inducer tip critical velocity ratio of 0.520, a linear decrease in hub-tip diameter ratio is exhibited in the range of specific speeds of 0.41 to 0.50. At the inducer tip critical velocity ratio of 0.346 this same decrease is noted in the specific speed range of 0.31 to 0.39. At the inducer tip critical velocity ratios of 0.693 and 1.212 the decrease is exhibited in the specific speed ranges of 0.59 to 0.68 and 0.79 to 1.01, respectively.

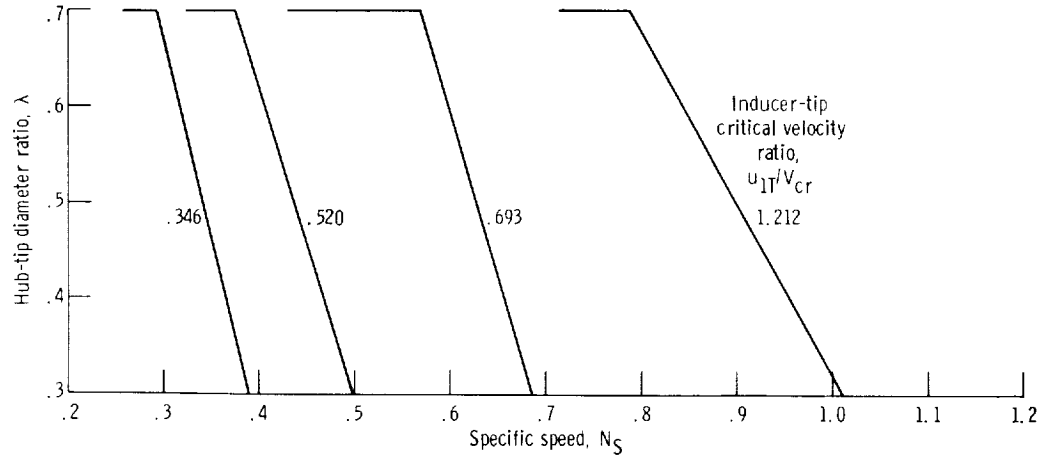

Figure 6. - Variation in optimum inducer hub-tip diameter ratio with specific speed at various inducer tip speeds.

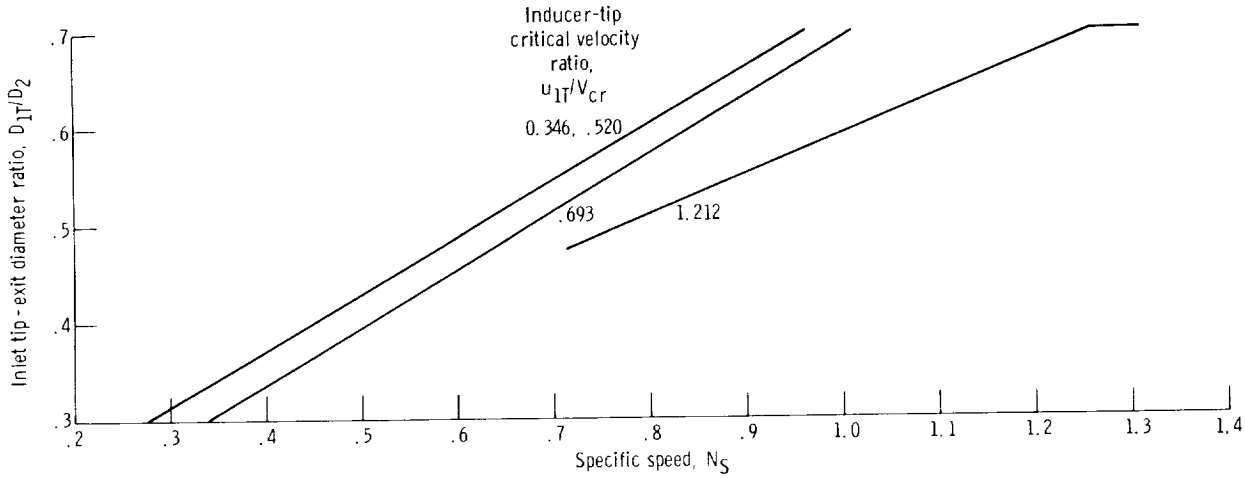

Figure 7. - Variation in optimum inlet tip-exit diameter ratio with specific speed for various inducer tip speeds.

The optimum inlet tip-exit diameter ratio is shown in figure 7. The low values at low specific speeds reflect the high ideal work relative to inlet flow volume that produces low specific speeds. This ratio increases linearly to the specified maximum at a specific speed of 0.95 for the inducer tip critical velocity ratios of 0.36 and 0.520. This characteristic curve was translated to higher specific speed values for the inducer tip critical velocity ratios of 0.693 and 1.212.

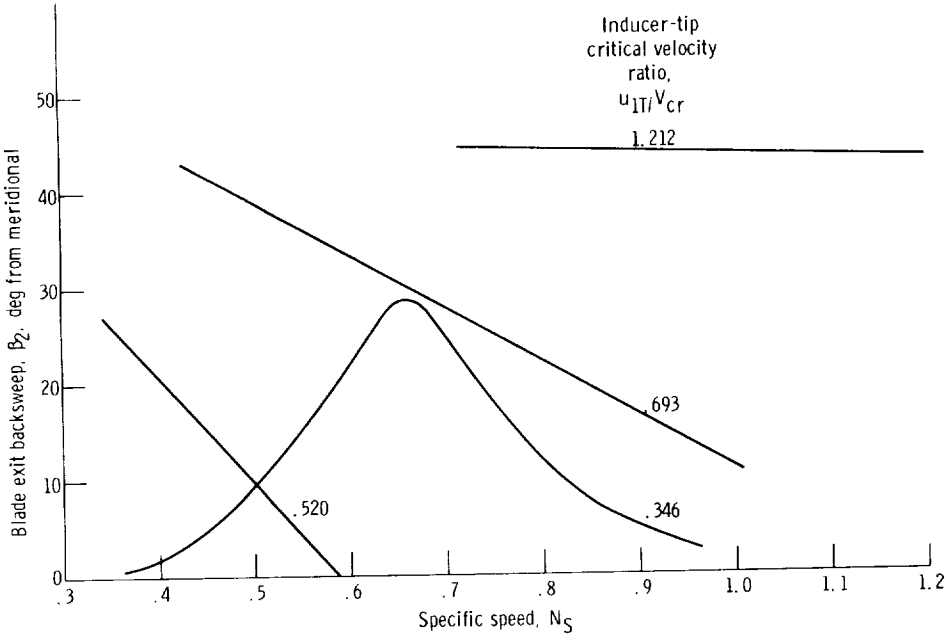

Figure 8. - Variation in optimum blade-exit backsweep with specific speeds at various inducer-tip speeds.

The variation in blade exit backsweep with specific speed for the four inducer tip speeds is shown in figure 8. Backsweep has a profound influence on impeller exit absolute Mach number reduction for a fixed-reaction rotor, so larger values of backsweep would be expected at lower specific speeds where higher absolute Mach numbers increase vaneless diffuser losses. However, for the impeller tip critical velocity ratio of 0.346 exit Mach numbers were near 0.8 maximum. This resulted in good vaned diffuser performance, and the improvements in diffuser pressure recovery attained with backsweep were negated by increased recirculation losses in the lower specific speed region where rotor exit absolute flow angles are large. In the higher specific speed range moderate backsweep was beneficial because recirculation losses were not significantly increased. For the inducer tip critical velocity ratio of 0.520 backsweep was beneficial up to specific speeds of 0.59. For the two higher inducer tip critical velocity ratios the impeller exit absolute Mach number was always greater than 0.8 and backswept impellers produced maximum total efficiency over the entire range of specific speeds investigated.

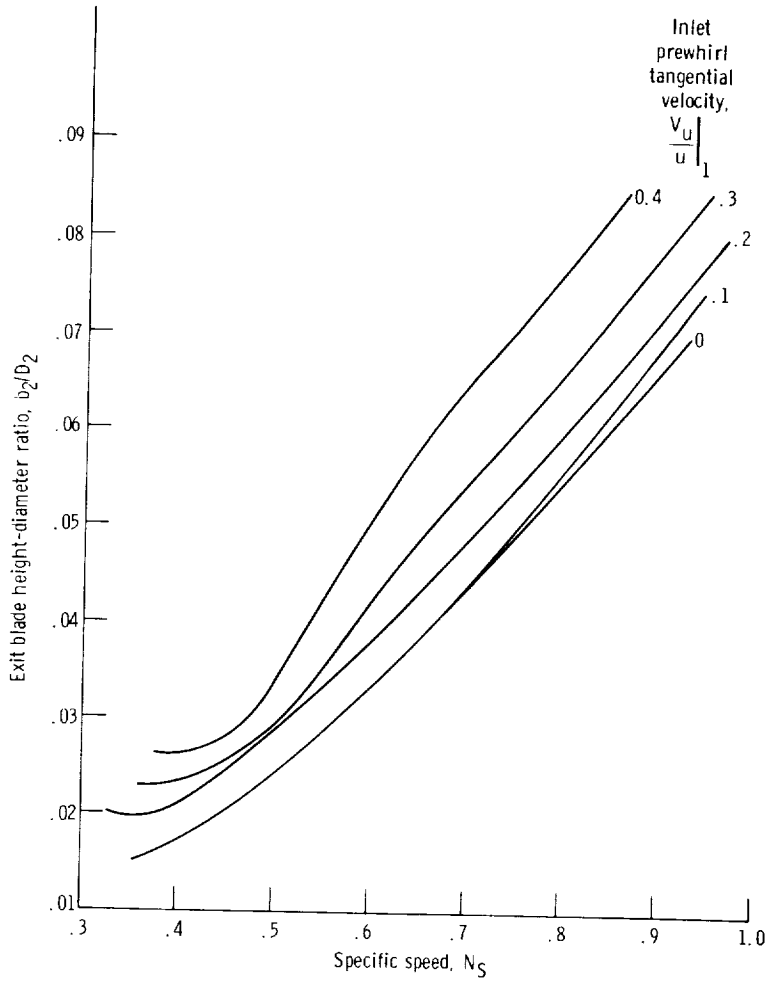

Figure 9. - Variation in optimum blade exit height-diameter ratio with specific speed at various inlet prewhirl tangential velocities.

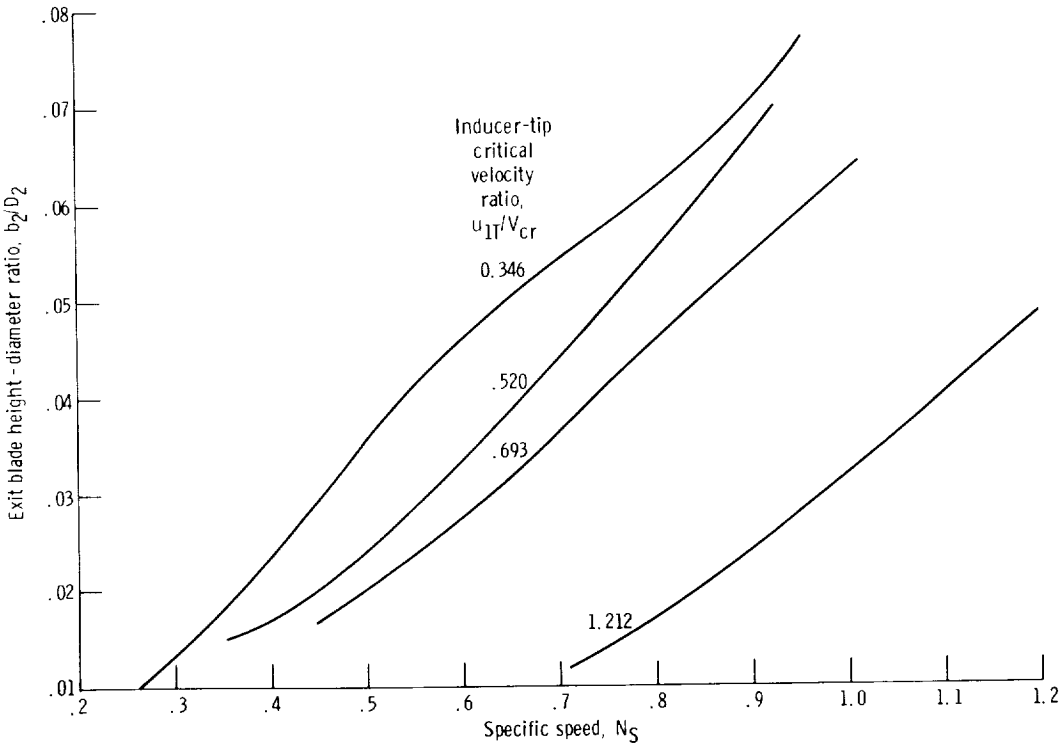

Figure 10. - Variation in optimum rotor exit blade height-diameter ratio with specific speed at various inducer tip speeds.

In the absence of a transonic loss correlation, compressor configurations with swirl-free inlets resulted in maximum total efficiency over the range of specific speeds investigated. If a correlation reflecting shock - boundary-layer interaction were included for configurations with transonic inducers, prewhirl would be expected to increase efficiency. However, prewhirl reduces the attainable pressure ratio for a given rotative speed and inlet tip-exit diameter ratio.

The ratio of exit blade height-diameter for maximum total efficiency is shown in figure 9 for a swirl-free inlet and four values of solid-body prewhirl at the inducer tip critical velocity ratio of 0.520. Increasing ratios with increasing specific speed reflect gas density decreases with compressor pressure ratio decreases. The effect of inducer tip speed on exit blade height-diameter ratio for the four configurations with swirl-free inlet only is shown in figure 10. Blade height decreases with increasing tip speed. This decrease is due to higher gas density and compressor pressure ratio associated with increased rotative speed.

Figure 11 shows the variation in compressor total pressure ratio for the four inducer tip speeds considered. The high-speed configuration had a transonic relative gas velocity at the inducer tip, and in the absence of transonic rotor losses the predicted attainable pressure ratio is obviously optimistic.

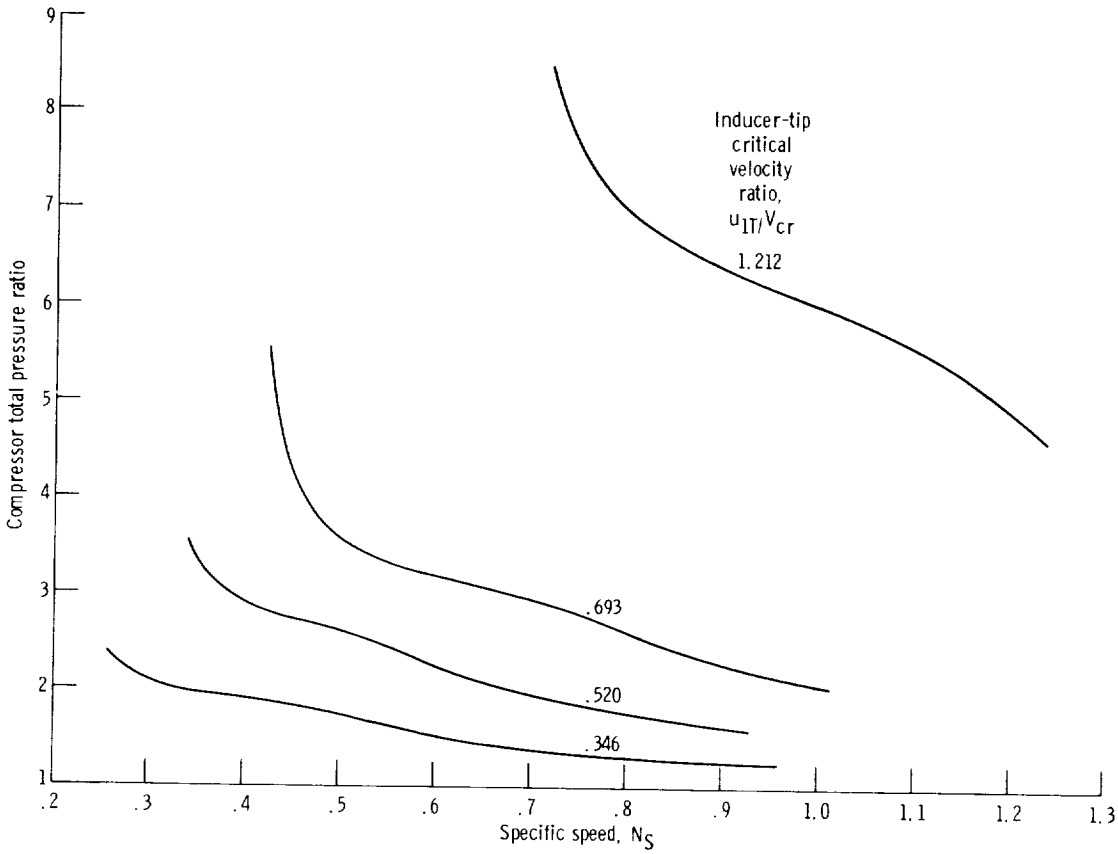

Figure 11. - Variation in compressor total pressure ratio for maximum total efficiency configuration with specific speed at various inducer tip speeds.

Loss Distribution

The distribution of internal losses along the curves of maximum total efficiency as a function of specific speed is shown in figure 12 for the four inducer tip speeds studied. The changes in loss distribution are shown to indicate the effect of internal velocity level on compressor performance. In the low range of specific speed attained by each inducer tip speed, the losses are dominated by disk friction and vaneless and vaned diffuser losses. Disk friction losses are large in the lower specific speed range because of the higher exit tip speeds and gas density that characterize low specific speed machines. Vaneless and vaned diffuser losses are large because of the higher impeller exit absolute Mach numbers associated with the lower specific speed machines. Skin friction loss, which was dependent on inducer inlet hub-tip diameter ratio, showed a marked change in level in the specific speed range where optimum inducer hub-tip diameter ratio changed for each tip speed.

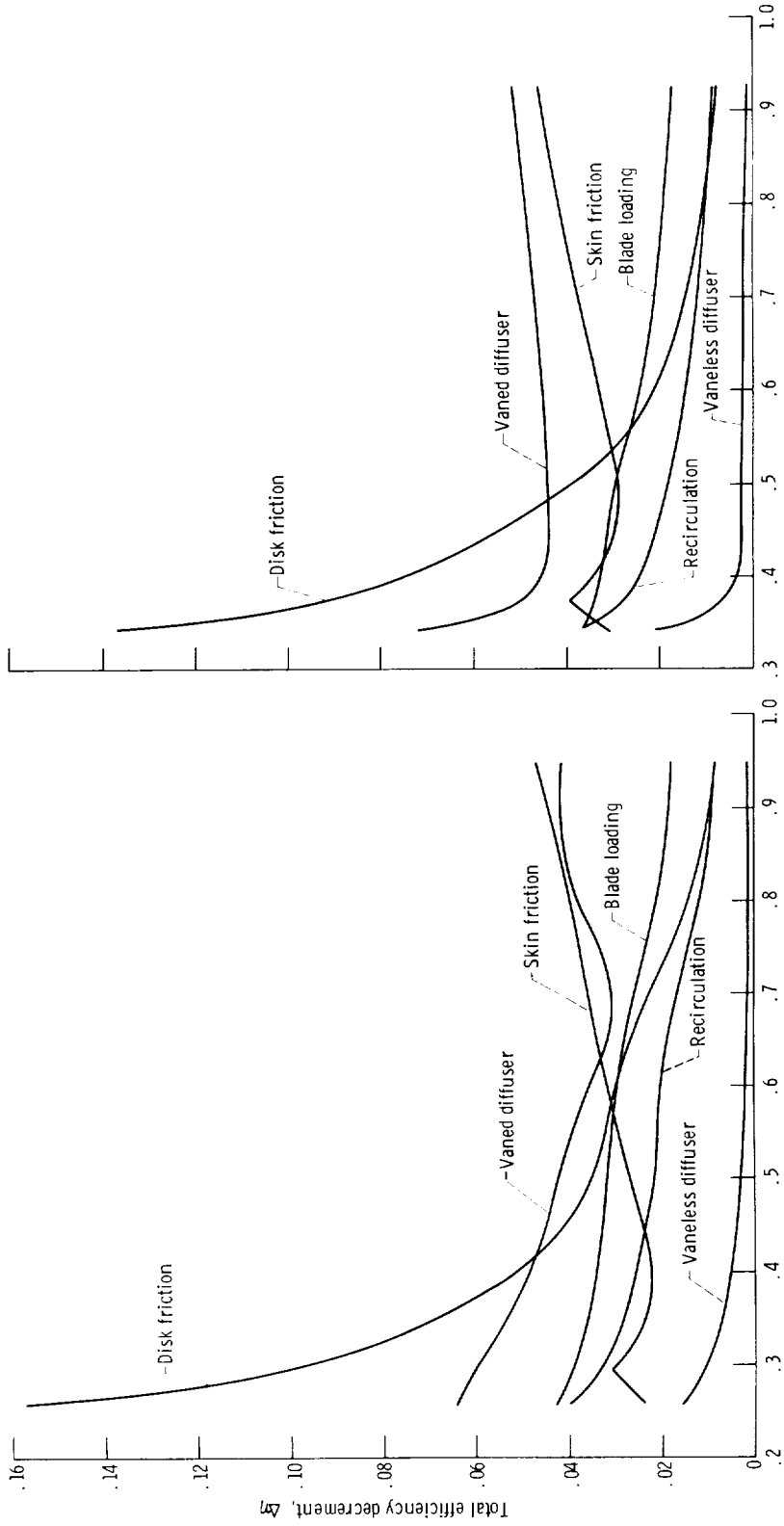

(a) Inducer tip critical velocity ratio, 0.346.

(b) Inducer tip critical velocity ratio, 0.520.

Figure 12. - Variation in internal loss distribution along curve of maximum total efficiency with specific speed.

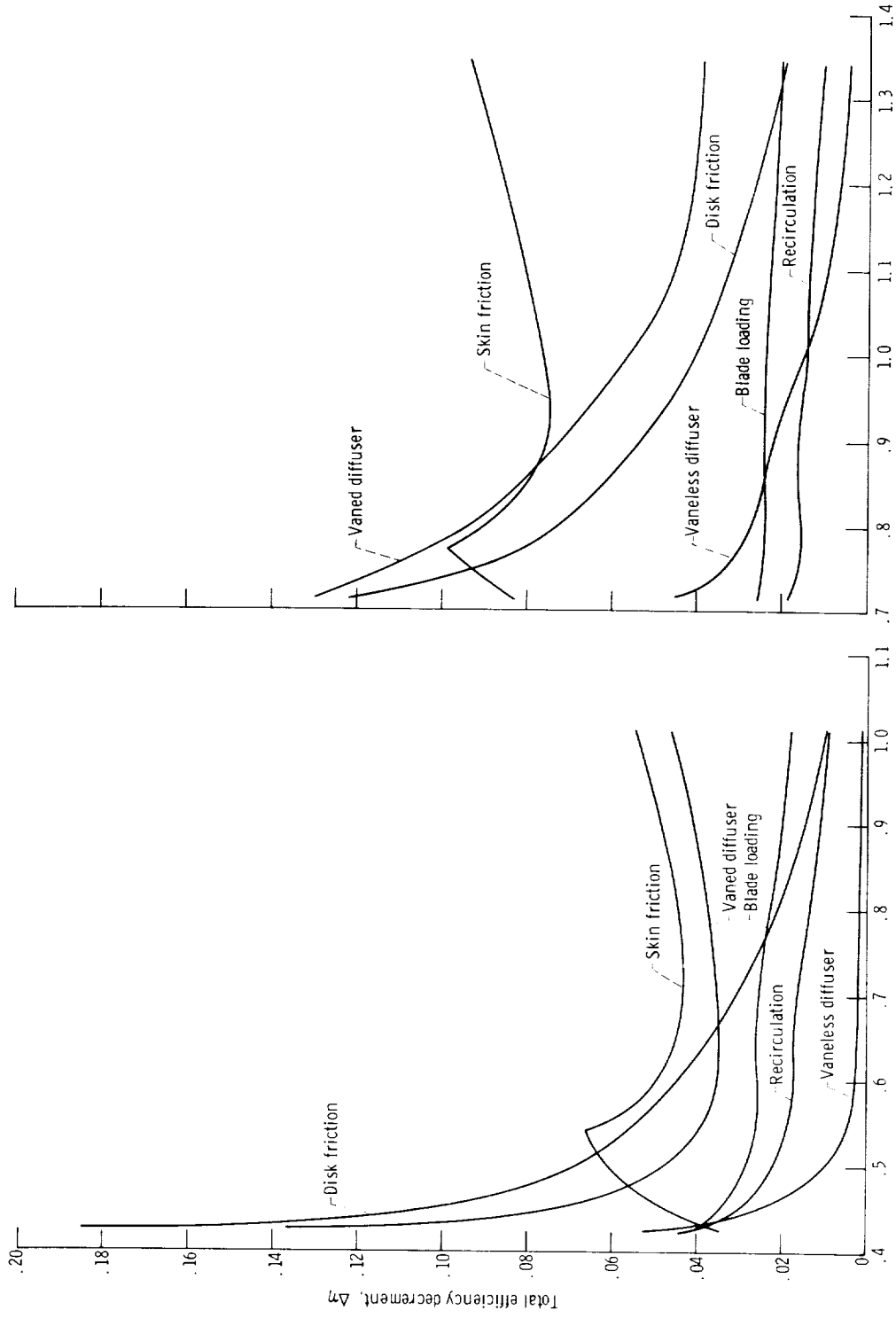

(c) Inducer tip critical velocity ratio, 0.693.

(d) Inducer tip critical velocity ratio, 1.212.

Figure 12. - Concluded.

Head Coefficient

The variation in head coefficient $\Delta H_{id}/u_2^2$ with specific speed and inducer tip speed is shown in figure 13. The variation in this parameter is included in addition to figure 11 because it permits a straightforward determination of impeller exit tip speed for a desired pressure ratio. The decrease in head coefficient in the mid-specific-speed range for the inducer tip critical velocity ratio of 0.346 is associated with the rapid change from radial to backswept impellers for maximum total efficiency. Efficiency is insensitive to backsweep in comparison to actual impeller work, thereby reducing head coefficient which is dependent on isentropic work.

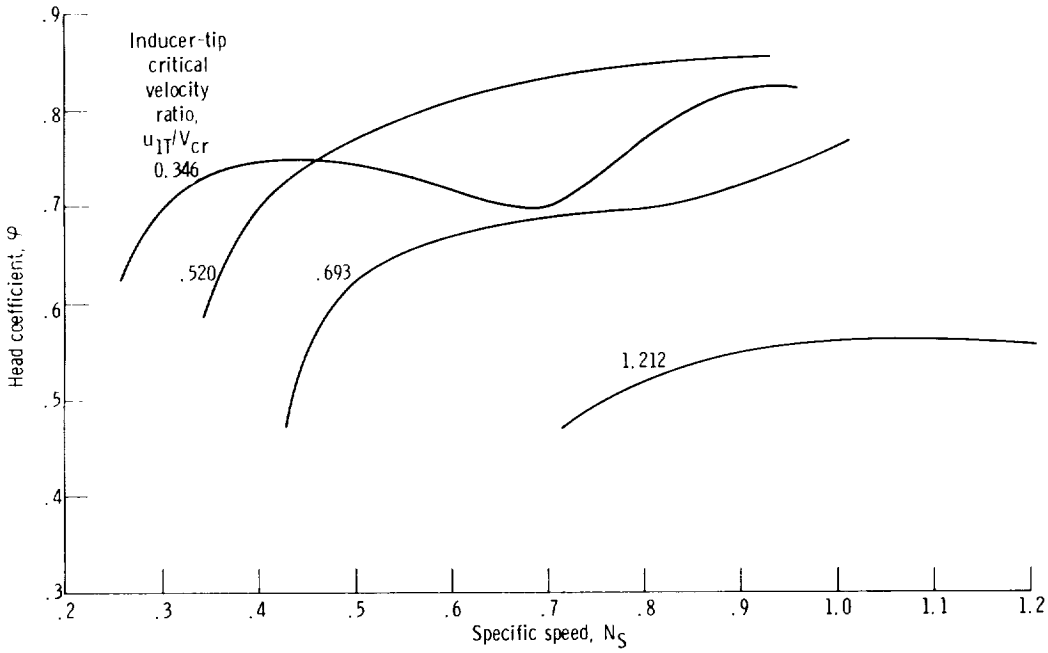

Figure 13. - Variation in optimum head coefficient with specific speed at various inducer tip speeds.

Application of Results

The results of this investigation provide a basis on which centrifugal compressors can be sized for applications in which maximum total efficiency is an important design parameter. Compressor specific speed can be estimated from desired rotative speed, pressure ratio, weight flow, and inlet density. When the approximate specific speed is known, figure 13 can be used to determine the rotor exit speed and, consequently, rotor exit diameter, and figures 6 and 7 can then be used to size the inlet. Then a new estimate

of specific speed can be made from the indicated volume flow rate required for the weight flow and inlet dimensions indicated. Several iterations of this procedure will determine compressor size for the application considered. Figures 4, 8, and 9 can then be used to determine impeller exit velocity diagram characteristics and geometry. Caution should be used with figures 6 and 9 because mechanical considerations are not reflected in these graphs. Severe inlet blockage problems may be encountered with low inlet hub-tip diameter ratios indicated in the high specific speed range. Actual exit blade height should be calculated from continuity at the rotor exit. The rotor exit velocity diagram can be constructed with the aid of figure 4, the wheel speed obtained from the use of figure 13, and the constraint placed on impeller exit-inlet tip relative velocity ratio. Impeller exit total temperature can be calculated from the actual aerodynamic work indicated by the impeller exit velocity triangle. Impeller exit total pressure can be estimated using a rotor efficiency computed with the aid of figure 12. Determination of the impeller exit absolute Mach number permits calculation of the exit static density. True blade height can then be calculated from the desired weight flow, the calculated static density, the indicated impeller exit diameter, and the absolute meridional velocity.

Hub and shroud contours and blade shape resulting in desirable diffusion may then be established by use of an internal velocity calculation program such as reference 10.

SUMMARY OF RESULTS

Centrifugal compressor geometry was examined analytically to determine the values of geometric variables that yield maximum total efficiency over a range of specific speeds. Geometric parameters considered were inlet hub-tip diameter ratio, inlet tip-exit diameter ratio, rotor exit blade height-exit diameter ratio, and blade exit backsweep. The variation of these values with specific speed was then determined, thereby providing a method by which low-loss geometry can be rapidly selected for any application in the range of specific speed investigation. The results of the analysis can be summarized as follows:

1. The flow conditions and geometric variables resulted in a specific speed range of 0.257 to 1.346 for the inducer tip speeds studied. Maximum total efficiencies ranged from 0.497 to 0.868.

2. Efficiency dropped rapidly with decreasing specific speeds in the lower specific speed range attainable by each inducer tip speed. This drop resulted from large losses associated with disk friction and both vaneless and vaned diffusers.

3. All of the geometric variables and velocity diagram characteristics studied were sensitive to changes in inducer tip speed.

4. Swirl-free inlet configurations resulted in maximum total efficiency in the range of specific speeds investigated. This resulted from a neglect of shock losses in the impeller.

Lewis Research Center,
National Aeronautics and Space Administration,
Cleveland, Ohio, December 21, 1972,
132-15.

APPENDIX A

SYMBOLS

a	local acoustic velocity, m/sec
B	diffuser effective depth ratio
b	blade height, m
C_f	skin friction coefficient
C_p	specific heat, J/(kg)(K)
C_p^{**}	maximum pressure recovery coefficient at a given area ratio
D	diameter, m
D_f	diffusion factor
e_s	inlet guide vane loss coefficient
H	overall ideal compressor enthalpy, J/kg
Δh	incremental compressor enthalpy, J/kg
L	blade length, m
M	Mach number
N_s	specific speed, dimensionless
p	pressure, N/m^2
Q	volume flow rate, m^3/sec
q	dimensionless enthalpy
R	gas constant, J/(kg)(K)
$\bar{R}$	radius ratio
Re	Reynolds number
r	radius, m
T	temperature
u	blade speed, m/sec
V	absolute gas velocity, m/sec
W	relative gas velocity, m/sec
w	mass flow rate, kg/sec

Z	number of blades
α	absolute flow angle, deg from meridional
β	relative flow angle, deg from meridional
β_b	blade angle, deg from meridional
γ	ratio of specific heats
δ	deviation angle between flow and blade
$\Delta\delta^*$	incremental boundary-layer displacement thickness, m
ζ	loss coefficient
η	efficiency
$\Delta\eta$	decrement in efficiency
λ	hub-tip diameter ratio
μ	dynamic viscosity, N-sec/m^2
ν	kinematic viscosity, m^2/sec
ρ	gas density, kg/m^3
φ	flow coefficient
ψ	head coefficient
ω	impeller angular velocity

Subscripts:

act	actual
aero	aerodynamic
av	average
BL	blade loading
calc	calculated
cr	critical condition
DF	disk friction
est	estimated
H	hub
hyd	hydraulic
IGV	inlet guide vane
i	iteration subscript

id	ideal
MF	root-mean-square
m	meridional
R	rotor
RC	recirculation
SF	skin friction
SL	slip
T	tip
th	theoretical
u	tangential
VD	vaned diffuser
VLD	vaneless diffuser
0	station just upstream of inlet guide vanes
1	impeller inlet
2	impeller exit
3	vaned diffuser inlet
4	vaned diffuser exit

Superscripts:

'	absolute stagnation
''	relative stagnation

APPENDIX B

EQUATIONS

The equations used in the calculation of compressor performance are listed here in the general order of solution. Several quantities were held constant for each set of calculations. These constants were inlet total conditions of the working fluid p_0' and T_0', fluid properties γ, R, and μ_0', and inducer tip speed μ_{1T}.

Geometric parameters D_{1T}/D_2, λ, Vu_{1T}, and β_{2b} were varied to obtain the range of specific speeds. Initial calculations were made at u_{1T}/V_{cr} of 0.52, and further investigations were performed at values of 0.346, 0.693, and 1.212 to study the effects of compressibility on compressor geometry and performance.

Impeller Inlet Velocity Triangles

For given values of V_{1T}/V_{cr} and prewhirl velocity at the impeller tip, relative velocity and meridional component of absolute velocity were calculated. With the solid body vortex prewhirl considered in this analysis, tangential components of absolute velocity were calculated by the relations

$$Vu_{1MF} = \left(\frac{D_{1MF}}{D_{1T}}\right) Vu_{1T} \tag{B1}$$

$$Vu_{1H} = Vu_{1T}\left(\frac{D_{1H}}{D_{1T}}\right) \tag{B2}$$

where D_{1MF} is the root-mean-square inlet diameter. Meridional component of absolute velocity must vary according to the relation (ref. 11)

$$V_{m1} = \sqrt{K - 2Vu_1^2} \tag{B3}$$

in order to satisfy radial equilibrium in a solid-body vortex. The constant in equation (B3) was evaluated at the tip since Vm_{1T} had been determined by the specified inlet critical velocity ratio and tip prewhirl velocity. With the constant known, absolute meridional components of velocity were calculated at the mean and hub. The inlet triangles were then determined from known wheel speeds and absolute velocity components.

Impeller Exit Velocity Diagram

At the impeller exit the flow was assumed to deviate from the blade with a slip velocity calculated by the equation from reference 3

$$V_{SL} = \frac{\sqrt{\cos \beta_{2b}}}{Z^{0.7}} u_2 \tag{B4}$$

where Z is the number of blades proposed by reference 12

$$Z = 6.5 \frac{D_2 + D_1}{D_2 - D_1} \cos\left(\frac{\beta_{1av} + \beta_{2b}}{2}\right) \tag{B5}$$

where

$$D_1 = \sqrt{0.5\left(D_{1T}^2 + D_{1H}^2\right)} \tag{B6}$$

The deviation angle between the blade and the flow is then specified by

$$\delta = \sin^{-1} \frac{V_{SL} \cos \beta_{2b}}{W_2} \tag{B7}$$

The other velocity diagram characteristics (see fig. 2) were calculated from the relations

$$Vm_2 = W_2 \cos (\beta_{2b} + \delta) \tag{B8}$$

$$V_{u2} = u_2 - V_{SL} - W_2 \cos (\beta_{2b} + \delta) \tan \beta_{2b} \tag{B9}$$

$$V_2 = \sqrt{Vu_2^2 + Vm_2^2} \tag{B10}$$

$$\alpha_2 = \tan^{-1}\left(\frac{Vu_2}{Vm_2}\right) \tag{B11}$$

$$u_2 = u_{1T}\left(\frac{D_2}{D_{1T}}\right) \tag{B12}$$

Inlet Guide Vane Loss

This loss was calculated using the equation

$$\Delta h_{IGV} = \frac{0.4}{2Re^{0.2}\cot\alpha_{1MF}}\left(V_0^2 + V_{1MF}^2\right) \tag{B13}$$

where

$$Re = \frac{w}{\mu D_{1T}}$$

Total pressure loss across the guide vanes was calculated by the method of reference 13, assuming that turbine stator loss coefficients could be applied to centrifugal compressor inlet guide vanes. The guide vane loss coefficient was calculated from the equation

$$e_s = \frac{0.0076}{\cos\alpha_{1MF} - 0.025}\left[1 + \frac{\cos\left(\frac{\alpha_{1MF}}{2}\right)}{0.7}\right] \tag{B14}$$

Ideal kinetic energy leaving the vanes was calculated by

$$(KE)_{id} = \frac{KE}{1 - e_s} \tag{B15}$$

where

$$KE = \frac{V_{1MF}^2}{2} \tag{B16}$$

Mean static temperature downstream of the inlet guide vanes was calculated from the equation

$$T_{1MF} = T_0' - \frac{V_{1MF}^2}{2C_p} \tag{B17}$$

The remaining fluid state conditions were computed from the relations:

$$\left(\frac{p}{p'}\right)_{1MF} = \left(1 - \frac{V_{1MF}^2}{2C_p T_0'}\right)^{\gamma/(\gamma-1)} \tag{B18}$$

$$\frac{p_{1MF}}{p_0'} = \left(1 - \frac{(KE)_{id}}{C_p T_0'}\right)^{\gamma/(\gamma-1)} \tag{B19}$$

$$p'_{1MF} = \frac{\left(\frac{p_{1MF}}{p_0'}\right)}{\left(\frac{p}{p'}\right)_{1MF}} p_0' \tag{B20}$$

$$p_{1MF} = p'_{1MF}\left(\frac{p}{p'}\right)_{1MF} \tag{B21}$$

$$\rho'_{1MF} = \frac{p'_{1MF}}{RT_0'} \tag{B22}$$

$$\rho_{1MF} = \rho'_{1MF}\left(\frac{p}{p'}\right)^{1/\gamma}_{1MF} \tag{B23}$$

$$\rho_0' = \frac{p_0'}{RT_0'} \tag{B24}$$

Velocity upstream of the inlet guide vanes was calculated by trial and error solution of the equation

$$\frac{\rho_0 V_0}{\rho_0' V_{cr}} = \left[1 - \frac{\gamma - 1}{\gamma + 1}\left(\frac{V_0}{V_{cr}}\right)^2\right]^{1/(\gamma-1)} \frac{V_0}{V_{cr}} \tag{B25}$$

where

$$\rho_0 V_0 = \rho_{1MF} V_{1MF} \cos \alpha_{1MF} \tag{B26}$$

Blade Loading Loss

The work loss due to blade loading was previously expressed as

$$\Delta h_{BL} = 0.05 D_f^2 u_2^2 \tag{B27}$$

as suggested by reference 6. Where the diffusion factor D_f was defined as

$$D_f = 0.3 + \frac{0.75\, q_{th}}{\frac{W_{1T}}{u_2}\left[\frac{Z}{\pi}\left(1 - \frac{D_{1T}}{D_2}\right) + 2\frac{D_{1T}}{D_2}\right]} \tag{B28}$$

for $W_2/W_{1T} = 0.7$

The dimensionless actual head was obtained from blade exit speed and absolute tangential velocity and rms inlet wheel speed and prewhirl velocity:

$$q_{th} = \frac{u_2 Vu_2 - u_{1MF} Vu_{1MF}}{u_2^2} \tag{B29}$$

Skin Friction Loss

Skin friction loss was found from the equation of reference 6:

$$\Delta h_{SF} = 5.6 C_f \frac{\left(\frac{L}{D_2}\right)}{\left(\frac{D_{hyd}}{D_2}\right)} \left(\frac{W}{u_2}\right)_{av}^2 u_2^2 \tag{B30}$$

where the mean flow path blade length-to-exit diameter ratio was expressed as

$$\frac{L}{D_2} = \frac{1}{2}\frac{1 - \frac{D_{1MF}}{0.3048}}{\cos \beta_{2b}} \tag{B31}$$

The ratio of mean hydraulic-to-exit diameter was found from the equation

$$\frac{D_{hyd}}{D_2} = \frac{1}{\frac{Z}{\pi \cos \beta_{2b}} + \frac{D_2}{b_2}} + \frac{\frac{D_{1T}}{D_2}}{\frac{2}{1-\lambda} + \frac{2Z}{\pi(1+\lambda)}\sqrt{1 + \tan^2 \beta_{1T}\left(\frac{1+\lambda^2}{2}\right)}} \tag{B32}$$

and the ratio of mean relative velocity-to-impeller exit velocity was determined by

$$\left(\frac{W}{u_2}\right)^2_{av} = \frac{1}{2}\left\{\left(\frac{Vm_{1MF}}{u_2}\right)^2 + \left(\frac{D_{1MF}}{D_2}\right)^2 + 0.49\left[\left(\frac{Vm_{1MF}}{u_2}\right)^2 + \left(\frac{D_{1T}}{D_2}\right)^2\right]\right\} \tag{B33}$$

since $W_2/W_{1T} = 0.7$

Recirculation Loss

The recirculation loss was simply a function of the exit absolute gas angle and impeller diffusion factor (ref. 6):

$$\Delta h_{RC} = 0.02(\tan \alpha_2)^{1/2} D_f^2 u_2^2 \tag{B34}$$

Disk Friction Loss

Impeller disk friction loss was computed with the equation of reference 7:

$$\Delta h_{DF} = 0.01356 \frac{\rho_2}{wRe^{0.2}} u_2^3 D_2^2 \tag{B35}$$

in which the weight flow rate w was calculated from the mean flow properties and inlet geometry

$$w = \frac{\pi}{4} D_{1T}^2 \left(1 - \lambda^2\right) \rho_{1MF} V_{1MF} \cos \alpha_{1MF} \tag{B36}$$

Reynolds number for this loss calculation was based on impeller exit dimensions and inlet stagnation conditions:

$$Re = \frac{u_2 D_2 \rho'_{1MF}}{\mu'_0} \tag{B37}$$

Calculation of the exit density required iterative computations. Exit density corresponding to an isentropic pressure rise across the rotor was chosen as a first approximitiation and the rotor adiabatic efficiency, which reflects blade loading, skin friction, and inlet guide vane losses, was calculated using the estimated value. The equations used in this procedure were as follows:

$$T''_{1MF} = T_{1MF} + \frac{W_{1MF}^2}{2C_p} \tag{B38}$$

$$T''_2 = T''_1 + \frac{u_2^2 - u_{1MF}^2}{2C_p} \tag{B39}$$

$$T_2 = T''_2 - \frac{W_2^2}{2C_p} \tag{B40}$$

$$T'_2 = T_2 + \frac{V_2^2}{2C_p} \tag{B41}$$

$$\Delta h_{act} = C_p T'_0 \left(\frac{T'_2}{T'_0} - 1 \right) \tag{B42}$$

$$\Delta h_{id} = \Delta h_{act} - \Delta h_{IGV} - \Delta h_{BL} - \Delta h_{SF} \tag{B43}$$

$$\eta_R = \frac{\Delta h_{id}}{\Delta h_{act}} \tag{B44}$$

$$p_2' = p_{1MF}' \left(\frac{\eta_R \, \Delta h_{act}}{C_p T_0'} + 1 \right)^{\gamma/(\gamma-1)} \tag{B45}$$

$$p_2 = \frac{p_2'}{\left(\frac{T_2'}{T_2} \right)^{\gamma/(\gamma-1)}} \tag{B46}$$

$$\rho_{2calc} = \frac{p_2}{RT_2} \tag{B47}$$

For subsequent iterations the calculated value of exit density was used as a new approximation, and the procedure was continued until estimated and calculated values agreed within 0.001.

Impeller Exit Geometry

Impeller exit blade height was calculated with the aid of the continuity equation. Blade height necessary to pass the calculated mass flow is

$$b_2 = \frac{w}{\pi \rho_2 D_2 V_{m2}} \tag{B48}$$

Vaneless Diffuser Loss

Vaneless diffuser radius ratio was determined by the restrictions on the Mach number entering the vaned diffuser. Vaned diffuser inlet Mach number was limited to 0.8 to guard against shock formation in the vaned diffuser. Because of the wide range of variables considered, the rotor exit absolute Mach number varied extensively. In cases where its value was less than or equal to 0.8, the vaneless space radius ratio was arbitrarily set at 1.02; in cases where its value was greater than 0.8, the radius ratio was

determined by the amount of diffusion necessary to reduce the Mach number to the specified limit.

Reference 8 developed differential equations relating Mach number, flow angle, and total temperature to vaneless diffuser radius ratio through the fundamental relations of continuity, meridional equilibrium, tangential equilibrium, heat transfer, and fluid state. Meridional equilibrium was satisfied by a balance of pressure forces, shear forces, and inertia forces. Tangential equilibrium was satisfied by a balance of shear forces and inertia forces. Combination of the equilibrium equations with continuity and state equations resulted in the equations relating the changes in Mach number and flow angle to changes in radius ratio.

Mach number and flow angle were calculated at increments of 0.02 in radius ratio by the numerical method described in detail in reference 8. The governing differential equations for adiabatic diffusion in a radial passage are

$$\frac{1}{M^2}\frac{dM^2}{d\bar{R}} = \frac{-2\left(1+\frac{\gamma-1}{2}M^2\right)}{M^2-\sec^2\alpha}\left[(\gamma M^2-\tan^2\alpha)\frac{\zeta}{B\cos\alpha}-\frac{1}{B}\frac{DB}{d\bar{R}}-\frac{\sec^2\alpha}{\bar{R}}\right] \tag{B49}$$

and

$$\frac{1}{\tan\alpha}\frac{d(\tan\alpha)}{d\bar{R}} = \frac{\sec^2\alpha}{M^2-\sec^2\alpha}\left\{\left[1+(\gamma-1)M^2\right]\frac{\zeta}{B\cos\alpha}-\frac{1}{B}\frac{dB}{d\bar{R}}-\frac{M^2}{\bar{R}}\right\} \tag{B50}$$

where

$$\zeta = \frac{C_f r_2}{b_2} \tag{B51}$$

$$\bar{R} = \frac{r}{r_2} \tag{B52}$$

$$B = \frac{b}{b_2} \tag{B53}$$

The schedule of effective passage depth was determined by boundary-layer displacement thickness growth on the end walls. The flow was assumed to follow a log-spiral path determined by the calculated angle along each increment in radius ratio. The incremental displacement thickness at each radius ratio was then calculated from the equation

$$\Delta\delta^* = \frac{0.37\ \Delta\bar{R}r_2}{8\cos\alpha}\left(\frac{V_2\ \Delta\bar{R}r_2}{\nu\cos\alpha}\right)^{-1/5} \tag{B54}$$

which is the displacement thickness predicted by the one-seventh power velocity distribution law discussed in reference 14.

The effective passage depth was then

$$B_{i+1} = B_i - \frac{2\ \Delta\delta^*}{b_2} \tag{B55}$$

and

$$\Delta B = B_i - B_{i+1} \tag{B56}$$

Loss in total pressure in the vaneless space was computed from the equation found in reference 5:

$$\frac{1}{\left(\frac{p_3'}{p_2'}\right)} = 1 + \frac{\gamma C_f}{\cos\alpha_2}\frac{r_2}{b_2}\frac{\int_1^R M^3\left(\frac{a}{a'}\right)\left(\frac{\rho}{\rho'}\right)\bar{R}\,d\bar{R}}{M_2\left(\frac{a}{a'}\right)_2\left(\frac{\rho}{\rho'}\right)_2} \tag{B57}$$

The integral in the above equation can readily be determined by numerical methods using the Mach number distribution calculated by equation (B49) and the familiar isentropic flow relations of reference 15. The radius ratio at which the vaned diffuser inlet Mach number restriction was satisfied was also assumed to be vaned diffuser throat. Throat static pressure was calculated from the equation

$$p_3 = \frac{p_3'}{\left(1 + \frac{\gamma - 1}{2}M_3^2\right)^{\gamma/(\gamma-1)}} \tag{B58}$$

Vaneless diffuser loss was then determined by

$$\Delta h_{VLD} = C_p T_2'\left[\left(\frac{p_3}{p_3'}\right)^{(\gamma-1)/\gamma} - \left(\frac{p_3}{p_2'}\right)^{(\gamma-1)/\gamma}\right] \tag{B59}$$

Vaned diffuser performance was predicted from test data reported in reference 9. Lines of maximum pressure recovery for a prescribed area ratio were estimated from the performance maps reported for single plane divergence diffusers with square throats. Throat conditions of total pressure, Mach number, and blockage were determined by the analysis of the vaneless diffuser. Vaned diffuser area ratio required to decelerate the flow to an exit Mach number of 0.2 was determined by iteration. Using the one-dimensional isentropic area ratio

$$AR = \frac{M_3}{0.2}\left[\frac{1 + \frac{\gamma - 1}{2}(0.2)^2}{1 + \frac{\gamma - 1}{2}M_3^2}\right]^{(\gamma+1)/2(\gamma-1)} \tag{B60}$$

as an initial guess, the maximum pressure recovery coefficient C_p^{**} corresponding to the throat Mach number, blockage, and area ratio was interpolated. Exit static and total pressures were then calculated from the pressure recovery coefficient and isentropic relation, respectively:

$$p_4 = C_p^{**}(p_3' - p_3) + p_3 \tag{B61}$$

$$p_4' = p_4\left[1 + \frac{\gamma - 1}{2}(0.2)^2\right]^{\gamma/(\gamma-1)} \tag{B62}$$

The subsequent approximations to the actual required area ratio are then a function of the previous approximation and the estimated and calculated exit total pressures:

$$AR_{i+1} = AR_i \frac{p_{4,i}'}{p_{4,i+1}'} \tag{B63}$$

The iteration was continued until two consecutive estimates of area ratio agreed within 0.001. When convergence was achieved, vaned diffuser loss was determined from the equation:

$$\Delta h_{VD} = C_p T_2'\left[\left(\frac{p_4}{p_4'}\right)^{(\gamma-1)/\gamma} - \left(\frac{p_4}{p_3'}\right)^{(\gamma-1)/\gamma}\right] \tag{B64}$$

Overall Efficiency

The overall adiabatic efficiency was calculated as follows:

$$\eta_{AD} = \frac{\Delta h_{aero} - \left(\Delta h_{IGV} + \Delta h_{BL} + \Delta h_{SF} + \Delta h_{VLD} + \Delta h_{VD}\right)}{\Delta h_{aero} + \Delta h_{DF} + \Delta h_{RC}} \tag{B65}$$

Efficiency Decrements

Decrements in efficiency caused by the individual losses were obtained as follows:

$$\Delta\eta_{IGV} = \frac{\Delta h_{IGV}}{h_{act}} \tag{B66}$$

$$\Delta\eta_{BL} = \frac{\Delta h_{BL}}{h_{act}} \tag{B67}$$

$$\Delta\eta_{SF} = \frac{\Delta h_{SF}}{h_{act}} \tag{B68}$$

$$\Delta\eta_{VLD} = \frac{\Delta h_{VLD}}{h_{act}} \tag{B69}$$

$$\Delta\eta_{VD} = \frac{\Delta h_{VD}}{h_{act}} \tag{B70}$$

$$\Delta\eta_{RC} = \frac{\Delta h_{RC}}{h_{act}} \tag{B71}$$

$$\Delta\eta_{DF} = \frac{\Delta h_{DF}}{h_{act}} \tag{B72}$$

where

$$h_{act} = \Delta h_{aero} + \Delta h_{DF} + \Delta h_{RC} \tag{B73}$$

Specific Speed

This term is defined as

$$N_s \equiv \frac{\omega \sqrt{Q_1}}{H_{id}^{3/4}} \tag{B74}$$

and is computed using

$$\omega = \frac{2u_{1T}}{D_{1T}} \tag{B75}$$

$$H_{id} = \eta_{AD}\left(u_2 Vu_2 - u_{1MF} Vu_{1MF}\right) \tag{B76}$$

$$Q_1 = \frac{\pi}{4} D_{1T}^2 \left(1 - \lambda^2\right) V_{1MF} \cos \alpha_{1MF} \tag{B77}$$

REFERENCES

1. Baljé, O. E.: A Study on Design Criteria and Matching of Turbomachines: Part B - Compressor and Pump Performance and Matching of Turbocomponents. J. Eng. Power, vol. 84, no. 1, Jan. 1962, pp. 103-114.
2. Nichols, K. E.; McPherson, D. G.; and Baljé, O. E.: Study of Turbine and Turbopump Design Parameters. Rep. S/TD 1735, Turbo Div, Sundstrand Corp., Nov. 20, 1959.
3. Wiesner, F. J.: A Review of Slip Factors for Centrifugal Impellers. J. Eng. Power, vol. 89, no. 4, Oct. 1967, pp. 558-572.
4. Stewart, Warner L.: A Study of Axial-Flow Turbine Efficiency Characteristics in Terms of Velocity Diagram Parameters. Paper 61-WA-37, ASME, Nov. 1961.
5. Dallenbach, F.: The Aerodynamic Design and Performance of Centrifugal and Mixed-Flow Compressors. Technical Progress Series. Vol. 3. SAE, 1961.
6. Coppage, J. E.; Dallenbach, F.; Eichenberger, J. P.; Hlavaka, G. E.; Knoernschild, E. M.; and Vanke, N.: Study of Supersonic Radial Compressors for Refrigeration and Pressurization Systems. AiResearch Mfg. Co. (WADC TR 55-257), Dec. 1956.
7. Shepherd, Dennis G.: Principles of Turbomachinery. Macmillan Co., 1956.
8. Stanitz, John D.: One-Dimensional Compressible Flow in Vaneless Diffusers of Radial- and Mixed-Flow Centrifugal Compressors, Including Effects of Friction, Heat Transfer, and Area Change. NACA TN 2610, 1952.
9. Runstadler, Peter W., Jr.: Pressure Recovery Performance of Straight-Channel, Single-Plane Divergence Diffusers at High Mach Numbers. Rep. N-88, Creare, Inc. (USAAVLABS-TR-69-56, AD-865300), Oct. 1969.
10. Katsanis, Theodore: Use of Arbitrary Quasi-Orthogonals for Calculating Flow Distribution in the Meridional Plane of a Turbomachine. NASA TN D-2546, 1964.
11. Vavra, Michael H.: Aero-Thermodynamics and Flow in Turbomachines. John Wiley & Sons, Inc., 1960.
12. Lazarkiewicz, Stephen; and Troskolanski, A. T.: Impeller Pumps. Pergamon Press, 1965.
13. Rohlik, Harold E.: Analytical Determination of Radial Inflow Turbine Design Geometry for Maximum Efficiency. NASA TN D-4384, 1968.

14. Schlichting, Hermann (J. Kestin, trans.): Boundary Layer Theory. Sixth ed., McGraw-Hill Book Co., Inc., 1968.

15. Shapiro, Ascher H.: The Dynamics and Thermodynamics of Compressible Fluid Flow. Vol. 1, Parts 1 and 2. Ronald Press Co., 1953.

NASA-Langley, 1972 —— 1 E-6638